Controlled propulsion in viscous fluids of magnetically actuated colloidal doublets

Pietro Tierno,* Oriol Güell, and Francesc Sagués
Departament de Química Física, Universitat de Barcelona, Martí i Franquès 1, 08028 Barcelona, Spain and Institut de Nanociència i Nanotecnologia IN2UB, Universitat de Barcelona, Barcelona, Spain

Ramin Golestanian
Department of Physics and Astronomy, University of Sheffield, Sheffield S3 7RH, United Kingdom

Ignacio Pagonabarraga
Departament de Física Fonamental, Universitat de Barcelona, Martí i Franquès 1, 08028 Barcelona, Spain and Institut de Nanociència i Nanotecnologia IN2UB, Universitat de Barcelona, Barcelona, Spain
(Received 2 July 2009; revised manuscript received 4 September 2009; published 8 January 2010)

We study the propulsion of a micron-size paramagnetic colloidal doublet dispersed in water and driven above a surface by an external precessing magnetic field. The applied field forces the doublet to precess around an axis parallel to the plane of motion and the rotation of the colloidal assembly is rectified into translation due to a periodic asymmetry in dissipation close to the bounding plate. These recent experimental findings [P. Tierno, R. Golestanian, I. Pagonabarraga, and F. Sagués, Phys. Rev. Lett. **101**, 218304 (2008)] are complemented here with a theoretical analysis of the system and extended to more complex magnetic modulations such as elliptical driving fields. Experimental results show a good agreement with numerical simulations with the aim to find the best conditions toward the optimization of propulsion speed and swimming efficiency.

DOI: 10.1103/PhysRevE.81.011402 PACS number(s): 82.70.Dd, 87.85.gj

I. INTRODUCTION

Swimming at low Reynolds number (Re) using a finite number of degrees of freedom requires subtle designs to break the time-reversible nature of the fluid flow [1,2]. For example, a system with one compact degree of freedom such as a scalloplike micro-object having a single hinge could never swim by periodically opening and closing its arms since it performs a reciprocal motion, i.e., a motion composed of periodic back and forward displacements, and it will exactly retrace its trajectory during each cycle. The same scallop would behave differently for high or intermediate Re, i.e., when inertia plays a role [4], or if the fluid is non-Newtonian [5]. As argued by Purcell in his seminal work [6], a necessary condition to achieve propulsion in a viscous Newtonian fluid is the presence of at least two independent degrees of freedom which describe a closed area in the configuration space.

There exist already a number of theoretical proposals for simple swimmers which exploit the minimal number of degrees of freedom. Among these, one can find model swimmers composed by three stiff arms [6–8], three spheres performing one-dimensional displacements [9–13], two spheres which exchange mass cyclically while changing their relative distance [14], or other configurations [15–21]. Accounting for flexibility in the swimmer, in its arms [22], tail [23] or body [4], constitutes a classic alternative strategy to avoid reciprocal motion.

Beside its fundamental motivation aimed to understand the underlying physics of microorganism motility, there is also a technological interest toward the fabrication of microscale swimmers which can navigate in a controlled way through small channels or porous media. These motivations have led to various experimental realizations of microscopic swimmers exhibiting usually flexible parts vibrated by using, for example, external magnetic fields [15,24–27]. Another class of realizations refers to chemically powered colloids where power is obtained by heterogeneous catalitic reactions on the colloidal surface, e.g., by using Pt-Au nanorods [28] or by producing Janus colloids [29]. Also excited surface waves [30] or electric field sources [31] have been used to propel artificial prototypes. Despite all these results, there are not many experimental realizations in the microscale of minimal swimmers which do not use flexible ends, probably due to the difficulty at such small scale to reproduce the theoretical predictions. We note that very recently this has been achieved by using colloidal particles in optical traps [32].

In our previous work [33], we have experimentally demonstrated a simple strategy to achieve propulsion of microobjects in water by using magnetically actuated colloidal doublets close to a solid surface. The doublets were made by linking two paramagnetic particles of different sizes with DNA bridges and were subjected to an external magnetic field precessing around an axis parallel to the plane of motion. This field forces the doublets to rotate close to the surface and these rotations create an asymmetry in friction, which is rectified into translation and net motion. The two degrees of freedom required by the Purcell scallop theorem are the doublet displacements parallel and perpendicular to the solid wall. This minimal microscale swimmer, which avoids deformations as opposed to all previously proposed model swimmers, was found stable over changes in experimental parameters and amenable to be extended to larger or longer particle assemblies [34].

*ptierno@ub.edu

Generalizing the study of Ref. [33], we analyze the specificity of propulsion induced by a bounding wall following a more comprehensive theoretical framework, and we derive an analytical expression for the propulsion speed of the rotating doublet. We discuss the effect of the hydrodynamic interactions between the particles composing the doublet and the asymptotic behavior of the swimmer velocity. We also explore both experimentally and theoretically how this mechanism of motion can be further improved by using, for example, more general magnetic modulations. In particular we vary the ellipticity of the applied magnetic field and show that the doublet velocity could be effectively increased in terms of this parameter.

In Sec. II we introduce the theoretical framework to describe the motion of the doublet and discuss the specificity of surface-induced displacement, as opposed to other types of swimming. In Sec. III we derive explicit analytical expressions for the translation velocity as a function of the director dynamics. Subsequently, in Sec. IV we analyze how the director which characterizes the doublet is coupled to the actuating magnetic field and obtain expressions for the mean doublet velocity, which we compare with experimental results. The results can be easily generalized to different types of actuating magnetic fields. We conclude by stressing the main results in Sec. V.

II. MODEL

Let us consider a doublet made of two spheres of radii R_a and R_b ($R_b=\gamma R_a$, $\gamma<1$) located at $\mathbf{r}_a$ and $\mathbf{r}_b$, respectively. The distance between the centers of these two spheres is kept fixed at $2L\equiv(R_a+R_b)=R_a(1+\gamma)$.

The center of mass of the doublet is placed at a distance h above a solid surface where the fluid satisfies stick boundary conditions. At low Re number, the linearity of the hydrodynamic equations allows one to relate the velocity of each colloidal sphere to the force acting on both of them,

$$\mathbf{v}_a=\mathbf{G}^{(a)}\cdot(\mathbf{1}-\mathbf{nn})\cdot\mathbf{F}^a+\mathbf{G}^{(a,b)}\cdot(\mathbf{1}-\mathbf{nn})\cdot\mathbf{F}^b,$$

$$\mathbf{v}_b=\mathbf{G}^{(a,b)}\cdot(\mathbf{1}-\mathbf{nn})\cdot\mathbf{F}^a+\mathbf{G}^{(b)}\cdot(\mathbf{1}-\mathbf{nn})\cdot\mathbf{F}^b, \qquad (1)$$

where $\mathbf{1}$ stands for the identity matrix, while $\mathbf{n}\equiv\frac{1}{2L}(\mathbf{r}_b-\mathbf{r}_a)$ denotes the director joining the two particle centers. In the previous equations the projection of the forces along the direction joining the two particles enforces the constraint which ensures that the doublet length does not change during its motion, $\mathbf{n}^2(t)=1$, and hence that the doublet does not suffer any internal deformation during its motion. It is easy to deduce that such a constraint force, say for particle a, is indeed $\mathbf{F}^c=\mathbf{nn}\cdot\mathbf{F}^a$, which implies that this force does not affect the doublet velocity. In the previous equations $\mathbf{G}^{(a,b)}\equiv\mathbf{G}(\mathbf{r}_a,\mathbf{r}_b)$ denotes the hydrodynamic mobility matrix which determines the flow at particle a generated by the force acting on colloid b. Accordingly, $\mathbf{G}^{(a)}\equiv\mathbf{G}(\mathbf{r}_a)$ is the mobility matrix of particle a. Since there is no net external force acting on the doublet, the total force has to vanish and accordingly, $\mathbf{F}^a+\mathbf{F}^b=0$. The spheres are paramagnetic and will respond to an applied magnetic field. Due to the doublet rigidity, we can describe the effect of the imposed magnetic field in terms of a unique characteristic force, associated with the stress the dipole is subjected to $\mathbf{F}\equiv\mathbf{F^b}=-\mathbf{F^a}$. Since we are interested in the motion of a colloidal doublet linked by DNA bridges, we can disregard the angular velocities and torques the individual particles are subjected to. Since the spherical particles are paramagnetic, it is not possible, in principle, to rotate them individually by applying a torque. Such a rotation would generate a net translation for an isolated colloid due to the hydrodynamic coupling between translation and rotation induced by the wall. However, in our case the doublet rotates as a result of the opposing forces acting on the two linked spheres.

Since the doublet performs a solid rigid motion, we can describe its displacement in terms of the rotation of the director which joins the particle centers, $\mathbf{n}$, and the displacement of a reference point along the line joining the two particles, $\mathbf{r}_0$. The latter is characterized by the fraction α, which partitions the distance between the particles,

$$\mathbf{r}_a=\mathbf{r}_0-2L\alpha\mathbf{n},$$

$$\mathbf{r}_b=\mathbf{r}_0+2L(1-\alpha)\mathbf{n}. \qquad (2)$$

Physically intuitive choices correspond to $\alpha=m_b/(m_a+m_b)$ when $\mathbf{r}_0$ reduces to the center of mass, $\mathbf{r}_{CM}$; $\alpha=1/2$, when $\mathbf{r}_0$ becomes the midpoint between the two particles; or $\alpha=R_b/(R_a+R_b)$, which corresponds to the doublet resistance center. In terms of these variables, the doublet motion reads

$$\dot{\mathbf{r}}_0=2L\{[1+(\mathbf{G}^{(a)}-\mathbf{G}^{(a,b)})(\mathbf{G}^{(b)}-\mathbf{G}^{(a,b)})^{-1}]^{-1}\cdot\dot{\mathbf{n}}-(1-\alpha)\dot{\mathbf{n}}\}. \qquad (3)$$

We are interested in actuated motion where the applied external field leads to periodic closed trajectories in the configuration space. For such trajectories, the average over a period gives $\langle\dot{\mathbf{n}}\rangle=0$, which implies that the mean doublet velocity, $\langle\dot{\mathbf{r}}_0\rangle$, does not depend functionally on the choice of the reference point to describe the doublet displacement.

The previous expressions show that the net motion of the doublet arises from the modification of the mobility matrices induced by the solid substrate. It will lead to a dependence of the self-mobility matrices $\mathbf{G}^{(a)}$ and $\mathbf{G}^{(b)}$ on the height of each colloid above the solid substrate, $h_{a(b)}$, and will also modify the flow that one colloid induces on its neighbor [35]. This latter effect is also present in the absence of a bounding wall, but in that case it does not give rise to a net doublet displacement; only the modification of the induced flow due to the bounding wall may result in a net translation. In this sense, the relevant contribution of this cross hydrodynamic coupling can be regarded of higher order than the direct colloid-wall mobility matrix if the distance of the doublet to the wall is large. The relative magnitude of the cross and self-mobilities will scale as $R_{a(b)}/2L$; hence, for elongated doublets away from each other the cross mobilities will be subdominant. In general, explicit expressions in powers of the relevant distances can be obtained when the doublet is far from the wall [36,37]. In our case, the separation between the two colloids is not too large, but for simplicity we will assume that the interaction of each particle with the solid substrate is dominant, and we will neglect the cross mobilities,

$\mathbf{G}^{(a,b)}$ and $\mathbf{G}^{(b,a)}$. We will show that this simplified approach captures the dominant hydrodynamic coupling of the colloids to the wall and the main properties of doublet motion and it provides quantitative agreement with the experimental results.

Assuming that the doublet propulsion velocity is determined essentially by the dynamic coupling of each colloid with the solid surface, we are left with the mobility matrix of an isolated sphere in the presence of a planar wall. In this case, the doublet average translational velocity reduces to

$$\langle \dot{\mathbf{r}}_0 \rangle = 2L\langle [1 + \mathbf{G}^a(\mathbf{G}^b)^{-1}]^{-1} \cdot \dot{\mathbf{n}} \rangle. \tag{4}$$

Due to the axisymmetric symmetry, the mobilities can be expressed in terms of two scalar functions, corresponding to displacements normal and parallel to the wall. Specifically,

$$\mathbf{G}^{(a)} = C_{\parallel}^{(a)}(\mathbf{r}_a)(1 - \hat{\mathbf{z}}\hat{\mathbf{z}}) + C_{\perp}^{(a)}(\mathbf{r}_a)\hat{\mathbf{z}}\hat{\mathbf{z}}. \tag{5}$$

The functions $C_{(\parallel,\perp)}^{(a)}(\mathbf{r}_a)$ depend nonlinearly on the distance to the wall. As a result, the trajectories of the two particles with time will lead to a time variation of both $\mathbf{n}$ and $\mathbf{r}_0$; the trajectory of the latter will be sensitive to the specific choice of the reference point to be tracked. A further simplification can be achieved if one selects the reference point such that its height remains invariant during the cyclic motion of the doublet. Using the axisymmetric nature of the mobility matrices and starting from Eq. (3) the variation in height of the reference point, $h_0 \equiv \hat{\mathbf{z}} \cdot \mathbf{r}_0$, can be expressed as

$$\dot{h}_0 = -2L\left[\frac{C_{\perp}^{(a)}}{C_{\perp}^{(a)} + C_{\perp}^{(b)}} - \alpha\right]\dot{n}_z. \tag{6}$$

Requiring $\dot{h}_0 = 0$ implies that $(1-\alpha)C_{\perp}^{(a)} = \alpha C_{\perp}^{(b)}$ must hold at any time, a condition which cannot be satisfied due to the nonlinear dependence of the mobilities on the time dependent particle positions. Therefore, at a finite distance above the wall it is not possible to get a value of α, showing that the doublet does not rotate around a fixed point, and that the joint displacements of $\mathbf{r}_0$ and $\mathbf{n}$ need to be resolved.

However, whenever the vertical displacements around the reference height are small, it is possible to linearize around a reference height, $\tilde{h}_0$. In this case, $\dot{h}_0$ is negligible if

$$1 \gg \left| \frac{C_{\perp}^{(a)}(\tilde{h}_0)}{C_{\perp}^{(a)}(\tilde{h}_0) + C_{\perp}^{(b)}(\tilde{h}_0)} - \alpha + (h_0 - \tilde{h}_0) \times \left[\frac{C_{\perp}^{(b)}(\tilde{h}_0)C_{\perp}^{(a)\prime}(\tilde{h}_0) - C_{\perp}^{(a)}(\tilde{h}_0)C_{\perp}^{(b)\prime}(\tilde{h}_0)}{[C_{\perp}^{(a)}(\tilde{h}_0) + C_{\perp}^{(b)}(\tilde{h}_0)]^2} \right] \right|. \tag{7}$$

The term proportional to the height deviation vanishes for $\tilde{h}_0 \to \infty$, while the difference between the first two terms vanishes if α corresponds to the resistance center. Although this result shows that the resistance center becomes asymptotically the natural reference point to characterize the doublet translation, even if we consider a different reference point, it is easy to verify that, away from the wall, the right-hand side is smaller than one. Hence, a generic reference point can provide a good approximation to the doublet motion.

The previous analysis indicates that the relevant reference variable which characterizes the displacement of a swimming object is sensitive to the particular mechanism which originates its motion. For simplified swimmers, whose motion is controlled by the relative motion of their parts in unbounded fluids, the center of resistance plays a central role since it is the point which evolves directly due to the crossed interaction between the moving parts, leading to the net displacement through hydrodynamic interactions [38]. The motion of a moving object with prescribed shape and variable surface velocity, in turn, is characterized through a surface average local velocity [39]. As opposed to these previous examples, for our doublet close to a bounding wall, the characteristic relevant translational velocity does depend on the details of the coupling to the bounding substrate.

III. PROPULSION VELOCITY

In view of the weak sensitivity of the swimmer translational velocity on the chosen reference point, we keep the choice of our previous papers [33,34] and analyze explicitly the translational velocity of the doublet by taking the center of mass as reference point. Using Eqs. (2), (3), and (5), the linear relation between the center-of-mass velocity, $\mathbf{V} \equiv \dot{\mathbf{r}}_{CM}$ and the doublet director reads

$$\mathbf{V} = \frac{2L}{1+\gamma^3}\left[\frac{-C_{\parallel}^{(a)} + \gamma^3 C_{\parallel}^{(b)}}{(C_{\parallel}^{(a)} + C_{\parallel}^{(b)})}(\mathbf{1} - \hat{\mathbf{z}}\hat{\mathbf{z}}) + \frac{-C_{\perp}^{(a)} + \gamma^3 C_{\perp}^{(b)}}{(C_{\perp}^{(a)} + C_{\perp}^{(b)})}\hat{\mathbf{z}}\hat{\mathbf{z}}\right] \cdot \frac{d\mathbf{n}}{dt}. \tag{8}$$

Although general expressions for the mobility matrices of isolated spheres in the presence of a plane wall are known and good approximations have been proposed to cover an arbitrary distance from the surface [35], we will carry out analytical analysis introducing the far-field approximation to the particle-surface mobility functions. The mobility matrices only depend on the height above the wall, $z_{a,b}$, and can be written as

$$C_{\parallel,\perp}^{(a)} = \frac{1}{6\pi\eta R_a}\left[1 - \alpha_{\parallel,\perp}\frac{9}{16}\frac{R_a}{z_a} + O\left(\frac{R_a}{z_a}\right)^3\right], \tag{9}$$

which can be expressed in terms of the center-of-mass height $h = \mathbf{r}_{CM} \cdot \hat{\mathbf{z}}$ and the doublet orientation making use of Eq. (2), which read for this particular choice,

$$\frac{z_{a(b)}}{R_a} = \frac{h}{R_a} \mp \frac{2L}{R_a(1+\gamma^{\mp 3})}n_z(t) \equiv \frac{h}{R_a} \mp \Lambda^{\mp} n_z.$$

In Eq. (9) η stands for the fluid viscosity, and the numerical coefficients $\alpha_{\parallel} = 1$ and $\alpha_{\perp} = 2$ account for the asymmetric motion induced by the wall at this lowest order of coupling. To leading order in the inverse separation from the solid wall, the center-of-mass velocity reads

$$\mathbf{V} = \frac{R_a \gamma}{(1+\gamma^3)} \frac{d\mathbf{n}}{dt} \cdot \left\{ \left[\gamma^2 - 1 - \frac{9}{16}(\gamma^2 - \gamma + 1)\left(\gamma \frac{R_a}{z_b} - \frac{R_a}{z_a} \right) \right] \times (\mathbf{1} - \hat{\mathbf{z}}\hat{\mathbf{z}}) + \left[\gamma^2 - 1 - \frac{9}{8}(\gamma^2 - \gamma + 1)\left(\gamma \frac{R_a}{z_b} - \frac{R_a}{z_a} \right) \right] \hat{\mathbf{z}}\hat{\mathbf{z}} \right\}. \tag{10}$$

The previous relation shows how the instantaneous doublet velocity changes as its orientation evolves in time. Before considering in detail how the dynamics of the director follows the rotating magnetic field, we can already analyze the center-of-mass velocity of the doublet as a function of the director trajectory in the synchronous regime, i.e., when the angle between the director and the field is constant. If the applied magnetic field precesses around an axis parallel to the solid substrate (which we take it to coincide with the y axis of an appropriately chosen coordinate system without lost of generality) with constant angular velocity Ω, the director will trace a closed orbit, which can be parametrized as

$$\mathbf{n}(t) = (\sin\theta \sin[\Omega t + \varphi], \cos\theta, \sin\theta \cos[\Omega t + \varphi]), \tag{11}$$

where we have introduced the opening angle of the director trajectory around the magnetic precessing axis, θ, and we have taken into account a dephasing φ with respect to the actuating magnetic field (where we have considered the origin of time such that the applied field points along the y direction).

The instantaneous velocity of the center of mass of the doublet parallel to the surface is derived as

$$V_x = \frac{R_a \gamma \Omega \sin\theta}{1+\gamma^3}\left[\gamma^2 - 1 - \frac{9}{16}(\gamma^2 - \gamma + 1)\left(\gamma \frac{R_a}{z_b} - \frac{R_a}{z_a} \right) \right] \times \cos(\Omega t + \varphi),$$

$$V_y = 0,$$

$$V_z = -\frac{R_a \gamma \Omega \sin\theta}{1+\gamma^3}\left[\gamma^2 - 1 - \frac{9}{8}(\gamma^2 - \gamma + 1)\left(\gamma \frac{R_a}{z_b} - \frac{R_a}{z_a} \right) \right] \times \sin(\Omega t + \varphi). \tag{12}$$

Averaging over one period, the only nonzero component corresponds to the velocity parallel to the plate in the direction perpendicular to the axis of rotation of the doublet,

$$\langle V_x \rangle = \frac{9 R_a \Omega}{16} \frac{\gamma(\gamma^2 - \gamma + 1)}{1+\gamma}\left[-\gamma - \frac{1}{\gamma^3} + \frac{\gamma}{\sqrt{1 - \left(\frac{R_a}{h}\Lambda^+ \sin\theta \right)^2}} + \frac{\gamma^{-3}}{\sqrt{1 - \left(\frac{R_a}{h}\Lambda^- \sin\theta \right)^2}} \right]. \tag{13}$$

For the particular case of a symmetric doublet, when $\gamma = 1$, the mean propulsion velocity simplifies to

$$\langle V_x \rangle = \frac{9}{16} R_a \Omega \left[-1 + \frac{1}{\sqrt{1 - \frac{R_a^2}{h^2}\sin^2\theta}} \right]. \tag{14}$$

The obtained mean propulsion velocity is consistent with the simple picture of a "rolling" displacement of the doublet along the surface very similar to a wheel rolling on a solid surface due to solid friction, where the enhanced friction coefficient of the particles near the wall surface plays the role of the no-slip solid friction. For a given precession orientation θ the propulsion velocity is proportional to a characteristic size of the doublet and the imposed rotation frequency.

IV. DIRECTOR DYNAMICS

We will next consider how the doublet director follows the rotating magnetic field. Such an analysis will clarify how the precession and dephasing angles will affect the doublet motion.

The colloidal particles composing the doublet are paramagnetic and thus acquire a moment $\mathbf{m} = V\chi\mathbf{H}$ when subjected to an external field $\mathbf{H}$, which points along the field direction. Here, χ is the volume magnetic susceptibility and V is the particle volume. To compute the magnetic moment of the doublet, we have to consider the correction due to the local dipolar field generated by the individual particles. Following Ref. [40], we obtain the total moment of the doublet as $\mathbf{m} = H\{(V_a\chi_a + V_b\chi_b)/[1 - (V_a\chi_a + V_b\chi_b)/(R_a + R_b)^3]\}\mathbf{n}_d$, where V_i and χ_i are the volume and magnetic susceptibility of the particles $i = a, b$ and $\mathbf{n}_d$ denotes the direction of the induced dipole. The dipole magnetic orientation relaxes toward the anisotropy doublet axis $\mathbf{n}$ on the Néel relaxation time scale. We restrict ourselves to the experimentally relevant regime where the director follows synchronously the external magnetic field, which corresponds to the situation where the internal relaxation is faster, and hence we can assume that the two relevant orientations coincide, $\mathbf{n}_d = \mathbf{n}$.

Hence, we can describe the director motion in terms of an overdamped dynamics, where the director angular velocity $\boldsymbol{\omega}$ is proportional to the magnetic torque $\mathbf{T}$ it experiences, namely,

$$\boldsymbol{\omega} = \frac{1}{\zeta_r}\mathbf{T} = \frac{\mu_0}{\zeta_r}\mathbf{m} \times \mathbf{H} = \frac{\mu_0 V_d H \chi}{\zeta_r}\mathbf{n} \times \mathbf{H}, \tag{15}$$

where we have introduced the effective rotational coefficient of the doublet, ζ_r, and the medium magnetic susceptibility μ_0. Consistently with the approximations in the previous section, we can disregard the position dependence of the rotation friction coefficient. The paramagnetic character of the particles implies that the magnitude of the induced moment can be tuned through the intensity of the applied magnetic field. The doublet director satisfies the kinematic equation,

$$\frac{d\mathbf{n}}{dt} = \boldsymbol{\omega} \times \mathbf{n}, \tag{16}$$

in terms of which we can write down explicitly

$$\frac{d\mathbf{n}}{dt} = \frac{\mu_0 V_d H \chi}{\zeta_r}\{\mathbf{H}(t) - \mathbf{n}(t)[\mathbf{n}(t) \cdot \mathbf{H}(t)]\}. \tag{17}$$

A. Circular rotating magnetic field

The rotating magnetic field can be decomposed as $\mathbf{H}(t)=\mathbf{H}_0+\mathbf{H}_1(t)$, where $\mathbf{H}_0\cdot\mathbf{H}_1=0$. It can be characterized by the inclination angle of the precessing axis with respect to an axis parallel to the solid substrate, ξ, such that $\tan\xi=H_1/H_0$. In the geometry described previously, consistent with the parametrization of the director kinematics [Eq. (11)], we represent the precessing magnetic field as $\mathbf{H}=(H_1\sin\Omega t, H_0, H_1\cos\Omega t)$. Inserting this expression in Eq. (17), we arrive at an explicit expression for the rotation angle of the doublet,

$$\cos^2\theta=\frac{1}{2}\left\{1-\left(\frac{\Omega_B}{\Omega\cos\xi}\right)^2+\sqrt{\left(\frac{2\Omega_B}{\Omega}\right)^2+\left[1-\left(\frac{\Omega_B}{\Omega\cos\xi}\right)^2\right]^2}\right\}, \quad (18)$$

expressed in terms of the characteristic frequency

$$\Omega_B=\frac{\mu_0 V_d H\chi H_0}{\zeta_r}, \quad (19)$$

which denotes the ratio between the magnetic torque and the fraction coefficient. The dephasing angle can be written down as

$$\tan\varphi=-\frac{\Omega}{\Omega_B}\cos\theta. \quad (20)$$

For small rotating frequencies, $\Omega/\Omega_B\ll 1$, the director follows essentially the precessing magnetic field. In fact, the director angle deviates quadratically in Ω/Ω_B initially. Namely,

$$\cos^2\theta\simeq\cos^2\xi\left[1+\left(\frac{\Omega}{\Omega_B}\cos\xi\sin\xi\right)^2\right]+\mathcal{O}\left(\frac{\Omega}{\Omega_B}\right)^4 \quad (21)$$

or, in terms of the angle,

$$\theta\simeq\xi-\frac{1}{2}\sin\xi\cos^3\xi\left(\frac{\Omega}{\Omega_B}\right)^2+\mathcal{O}\left(\frac{\Omega}{\Omega_B}\right)^4. \quad (22)$$

In this regime, the director moves in phase, lagging slightly behind the magnetic field, since

$$\tan\varphi\simeq-\frac{\Omega}{\Omega_B}\cos\xi\left[1+\frac{1}{2}\left(\cos\xi\sin\xi\frac{\Omega}{\Omega_B}\right)^2\right]+\mathcal{O}\left(\frac{\Omega}{\Omega_B}\right)^5, \quad (23)$$

which in terms of the angle reads

$$\varphi\simeq-\frac{\Omega}{\Omega_B}\cos\xi\left[1+\frac{3\sin^2\xi-2}{6}\frac{\Omega^2}{\Omega_B^2}\cos^2\xi\right]+\mathcal{O}\left(\frac{\Omega}{\Omega_B}\right)^5. \quad (24)$$

The weak dependence on the rotating frequency implies that in this regime the director can essentially follow the external magnetic field.

The situation changes at high frequencies. As the frequency increases beyond the characteristic doublet angular velocity, the doublet shows a larger difficulty to follow the actuating magnetic field. As a result, its angle starts to decrease and finally will become parallel to the y axis. In the high-frequency regime, when $\Omega/\Omega_B\gg 1$,

$$\cos^2\theta\simeq 1-\left(\frac{\Omega_B}{\Omega}\tan\xi\right)^2+\mathcal{O}\left(\frac{\Omega_B}{\Omega}\right)^4, \quad (25)$$

in terms of the precessing angle, reads $\theta\simeq\tan\xi\Omega_B/\Omega+\mathcal{O}((\Omega_B/\Omega)^3)$.

The dephasing angle increases at high frequencies, and the director tends asymptotically to lag in quadrature with the magnetic field, namely,

$$\tan\varphi\simeq-\frac{\Omega}{\Omega_B}\left[1-\frac{1}{2}\left(\frac{\Omega_B\tan\xi}{\Omega}\right)^2\right]+\mathcal{O}\left(\frac{\Omega_B}{\Omega}\right)^3, \quad (26)$$

which in terms of the angle reads

$$\varphi\simeq-\frac{\pi}{2}+\frac{\Omega_B}{\Omega}+\left(\frac{5}{6}+\frac{1}{2\cos^2\xi}\right)\left(\frac{\Omega_B}{\Omega}\right)^3+\mathcal{O}\left(\frac{\Omega_B}{\Omega}\right)^5, \quad (27)$$

showing that to leading order the magnetic field does not affect the doublet quadrature lagging.

The intrinsic frequency makes it possible to identify a characteristic doublet velocity scale, $V_0=\frac{9}{16}\{[\gamma(\gamma^2-\gamma+1)]/(1+\gamma)\}R_a\Omega_B$, in terms of which the mean doublet velocity, Eq. (13), reduces to

$$\frac{\langle V_x\rangle}{V_0}=-\frac{\Omega}{\Omega_B}\left[\gamma+\frac{1}{\gamma^3}-\frac{\gamma}{\sqrt{1-\left(\frac{R_a\Lambda^+\sin\theta}{h}\right)^2}}-\frac{\gamma^{-3}}{\sqrt{1-\left(\frac{R_a\Lambda^-\sin\theta}{h}\right)^2}}\right]. \quad (28)$$

The magnitude of the characteristic velocity V_0 can be tuned by modifying the strength of the applied magnetic field, because the magnitude of the induced dipole depends on the field itself. The magnitude of the applied field does not affect the other features of the doublet velocity. Both the precessing angle and the dephasing with respect to the actuating field depend on the dimensionless frequency Ω/Ω_B and the precession angle of the magnetic field. The previous expression shows that, for a given magnetic intensity, these are the only two relevant parameters determining the motion of the doublet.

To experimentally realize the colloidal doublets we have used paramagnetic particles coated with streptavidin with two different radii, $R_a=1.4$ μm and $R_b=0.5$ μm (Dynabeads). As values for the magnetic volume susceptibilities of the two particles we have used $\chi_a=0.4$ [41] and $\chi_b=1.1$ [42]. The particles were linked with two complementary DNA strands (25 bp, 8 nm long) following the procedure outlined in the supporting information of Refs. [33,43]. The doublets have been dispersed in Millipore water and deposited above a clean glass plate. After ~5 min the doublets sediment above the plate and float at an elevation h due to electrostatic repulsive interactions. The glass plate acquires a negative

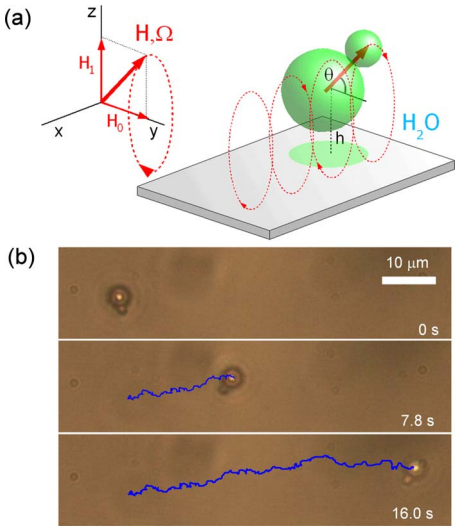

FIG. 1. (Color online) (a) Scheme showing a paramagnetic doublet floating above a glass plate (distance from center of mass h) and subjected to an external magnetic field H precessing around the y axis with frequency Ω. θ denotes the angle that the doublet director makes with the y axis and H_0, H_1 the field components along the y and z axes. (b) Microscope images taken at different times of a doublet traveling with a speed of ~ 3 μm/s. Superimposed is the particle trajectory after 7.8 and 16.0 s. In [3] the corresponding video file is deposited.

charge in water due to the dissociation of the silanol groups [44]. The paramagnetic doublets also acquire a double layer due to the negatively charged streptavidin located at the surface of the particles. The balance between gravity and electrostatic interactions confines the doublets, which show a diffusion predominantly in the (x,y) direction and diffusion coefficient $D=0.06\pm0.01$ μm^2/s, as estimated from the mean-square displacement (not shown here). The external magnetic field is provided by using three custom-made coils perpendicular to each other and having the main axes along the (x,y,z) directions.

In Fig. 1(b) we show three microscope images taken at different times (0, 7.8, and 16.0 s) of a paramagnetic doublet subjected to an external magnetic field having $H_0/H_1=0.27$ and $\Omega=81.7$ s^{-1}. After 16 s the doublet covers a distance of ~ 54 μm following almost a linear trajectory. Small deviations from a straight line are due to Brownian forces which are capable to slightly perturb the linear motion over times larger than Ω^{-1}.

In Fig. 2 we show the scaled doublet velocity V/V_0 as a function of Ω/Ω_B [with an error bar $\delta(V/V_0)=0.1$] for a doublet subjected to a magnetic field with precession angle $H_0/H_1=0.27$. The experimental points are represented by open circles while the continuous line is a theoretical fit made by using Eq. (28). From the fit we estimate the elevation h of the doublet from the plate to be $h=2.05$ μm and the rotational friction coefficient $\zeta_r=8.6\times10^{-19}$ N s m, which enters into the expression of Ω_B. The agreement between the theory and the experimental data is very good. At small rotating frequencies, the change in the precessing angle is subdominant because, as we have shown, the change in precessing angle is quadratic in the magnetic field frequency.

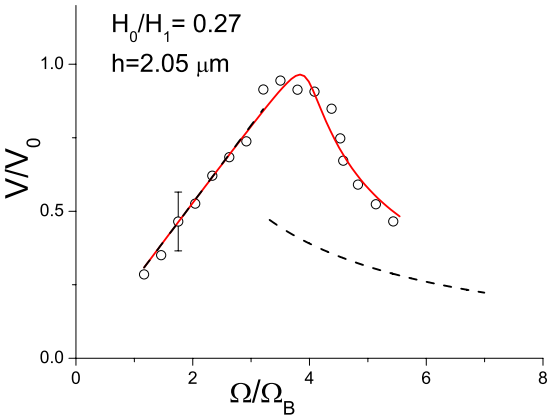

FIG. 2. (Color online) Scaled doublet velocity V/V_0 as a function of the normalized frequency Ω/Ω_B for $H_0/H_1=0.27$ and $h=2.05$ μm. The experimental data (open circles) are plotted together with a nonlinear curve fit (continuous line) and Eqs. (29) and (30) for the limits $\Omega/\Omega_B\to0$ and $\Omega/\Omega_B\to\infty$ (dashed lines), respectively.

Hence, the initial increase in the swimming velocity is linear,

$$\frac{\langle V_x\rangle}{V_0}\simeq-\frac{\Omega}{\Omega_B}\left[\gamma+\frac{1}{\gamma^3}-\frac{\gamma}{\sqrt{1-\left(\frac{R_a\Lambda^+\sin\xi}{h}\right)^2}}-\frac{\gamma^{-3}}{\sqrt{1-\left(\frac{R_a\Lambda^-\sin\xi}{h}\right)^2}}\right]+\mathcal{O}\left(\frac{\Omega}{\Omega_B}\right)^3. \quad (29)$$

The dashed line in Fig. 2 shows this asymptotic behavior for $\Omega/\Omega_B<3$. The asymptotic expression capture well the dependency of the speed on the external frequency.

In the limit of large frequencies the doublet precessing angle starts decreasing. This leads to a corresponding decrease in the velocity at which the doublet displaces, which decays asymptotically to zero as

$$\frac{\langle V_x\rangle}{V_0}\simeq\frac{\gamma(1+\gamma^2)}{2}(\Lambda^+)^2\frac{\Omega_B}{\Omega}\left(\frac{R_a}{h}\tan\xi\right)^2+\mathcal{O}\left(\frac{\Omega_B}{\Omega}\right)^3. \quad (30)$$

This limit is illustrated in Fig. 2 by the second dashed line for $\Omega/\Omega_B>3$, showing that the asymptotic will be reached at high frequencies. However, it was not possible to measure the doublet speed at frequencies higher than $\Omega\sim6\Omega_B$ and thus to test the second asymptotic limit. This is because at large frequencies of the external field asynchronous motion of the rotating doublet occurs which lead to a further reduction in the doublet motion.

Figure 2 shows that the doublet motion is characterized by two different dynamic regimes. A first regime appears at low frequencies, where the doublet essentially follows the actuating field, and where its velocity increases linearly with the rotating frequency of the field. Such a linear dependence is expected since we are operating the doublet in the low Re regime. At high enough frequencies, the doublet cannot follow the rotation frequency of the field. In the synchronous

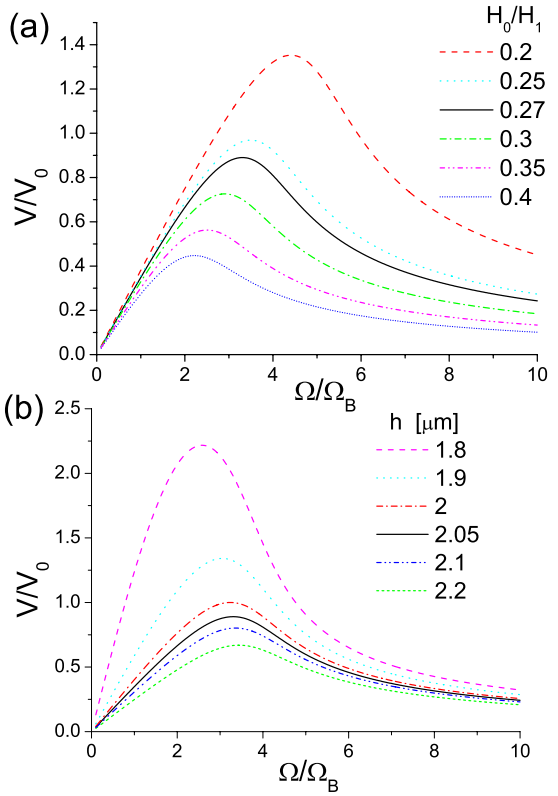

FIG. 3. (Color online) Scaled doublet velocity V/V_0 as a function of the normalized frequency Ω/Ω_B (a) for different precession ratios H_0/H_1 with $h=2.05$ μm and (b) for different distances from the wall h with $H_0/H_1=0.27$.

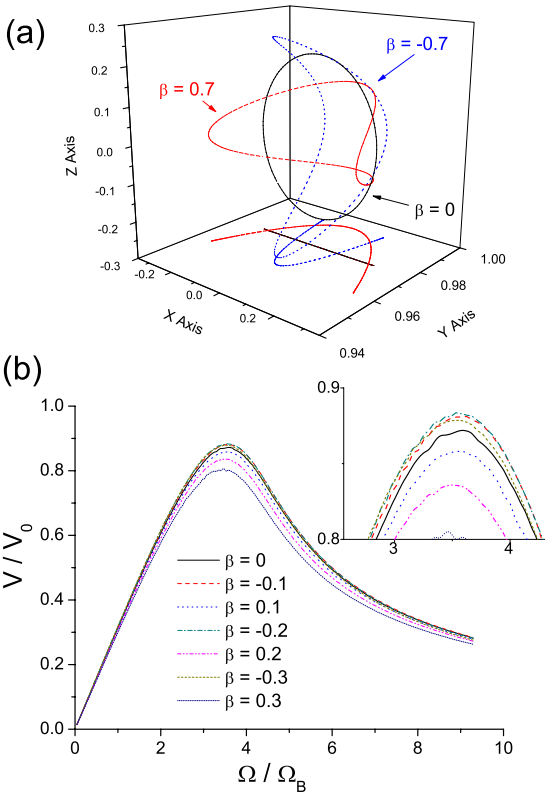

FIG. 4. (Color online) (a) Representation in the three-dimensional space of the director tip trajectories for different ellipticity parameters, $\beta=-0.7$, 0, and 0.7. (b) Scaled doublet velocity as a function of Ω/Ω_B for different values of β. The upper inset shows an enlargement of the graphs close to the velocity maximum with $H_0/H_1=0.27$ and $h=2.05$ μm.

regime the doublet precessing angle starts to decrease and the doublet lags behind the forcing field. The effective velocity of the doublet then decays and vanishes at high enough frequencies because the doublet aligns parallel to the substrate wall.

To elucidate the dependence of the doublet velocity from the various system parameters, we have plotted Eq. (28) in Fig. 3 for different precessing ratios of the magnetic field H_0/H_1 [Fig. 3(a)] and different distances from the surface h [Fig. 3(b)]. In both images the continuous lines refer to the experimental conditions with $h=2.05$ μm and $H_0/H_1=0.27$. From the first graph it follows that decreasing the precession ratio increases the peak of the curve while shifting it toward the higher frequencies. Lower precession ratios of the applied magnetic field correspond to higher precession angles θ of the doublet and thus to rotations closer to the surface. Such trajectories enforce the friction asymmetry during each cycle and increase the rate of rectification into motion i.e., the doublet speed. The effect of the plate on the doublet motion is clearly evidenced in Fig. 3(b) where small changes in the doublet elevation produce large variation in the peak speed of the doublets. We note also that decreasing h slightly shifts the speed peak toward the lower frequencies and induces a faster decrease as the frequency increases.

B. Elliptical rotating magnetic field

We consider here an extension of our model for the case when the external magnetic field is elliptically polarized in the (x,z) plane. This gives a different behavior from the circular magnetic field since the displacements of the small particle along x and z axes are not equivalent due to the presence of the plane. The external magnetic field can be written in terms of the ellipticity parameter β as [45] $\mathbf{H}(t)=(H_1\sqrt{1+\beta}\sin\Omega t, H_0, H_1\sqrt{1-\beta}\cos\Omega t)$. The director dynamics can be found by numerically solving Eq. (17), and the results are shown for one field cycle in Fig. 4(a) for a circular magnetic field ($\beta=0$) and two elliptically polarized fields with $\beta=-0.7$ and 0.7. When $\beta\neq 0$, the director $\mathbf{n}$ is forced to describe a curved trajectory in the plane (z,y) since it has to satisfy at any point the condition $|\mathbf{n}|=1$. The projection of the director dynamics along the (x,y) plane is represented by a line for a circular field $\beta=0$ and two opposite parabolic trajectories for $\beta=\pm 0.7$. Depending on the ellipticity β, the doublet acquires different velocities. In Fig. 4(b) we show the normalized doublet velocity V/V_0 as a function of the scaled frequency Ω/Ω_B for four different magnitudes of β.

Almost all curves follow the same trend at small frequencies ($\Omega<3\Omega_B$), while they differ at large frequencies. The peak velocity is higher for negative ellipticity values with a peak velocity $V_p=0.88V_0$ at $\beta=-0.2$, which corresponds to a speed of ~ 3 μm/s. This is reasonable since decreasing β the small particle rotates closer to the bounding plate following this curved asymmetric trajectory. Moreover, increasing

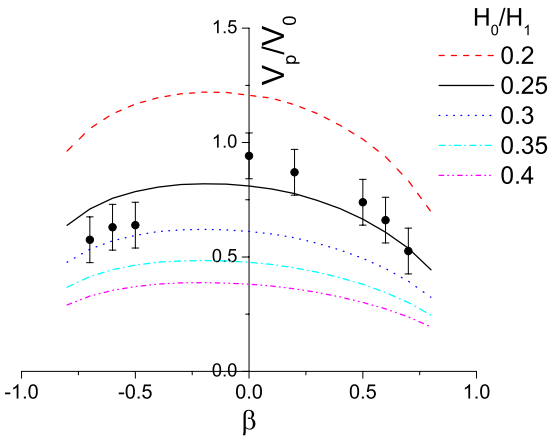

FIG. 5. (Color online) Scaled peak velocity V_p of the doublet as a function of the ellipticity parameter for different precession ratios H_0/H_1 with $h=2.05$ μm. The experimental points (closed circles) refer to a ratio $H_0/H_1=0.25$.

the magnitude of β decreases the area described by the doublet and its efficiency in rectification since in the limit $\beta=\pm 1$ the doublet would not further move. To characterize the doublet motion when subjected to an elliptically polarized magnetic field, we numerically calculate the peak velocities V_p for different ratios H_0/H_1 and plot them as a function of β in Fig. 5 for a fixed frequency of $\Omega=62.8$ s^{-1}. Together with the theoretical values (continuous line) we show experimental points (filled circles) taken by using the setup of Ref. [34] and under the conditions of $H_0/H_1=0.25$. The peak velocity decreases by increasing the field ellipticity for both signs and stops when $\beta=1$. The asymmetric dependence with positive and negative values of the ellipticity β reflects how the rotating colloid feels the asymmetry in friction coupling to the wall. The discrepancy between the experimental points and theoretical curves in Fig. 5 could be due to various effects. Our analysis, which considers the predominant magnetic and hydrodynamic interactions did not account for other smaller effects arising from electrostatic and steric interactions between the particle and the plane. Such interactions, which are more difficult to consider due to unknown parameters such us surface charge and thickness of the DNA chains covering the particle, can affect the particle motion but fall inside the experimental errors of our measurements. In this respect we notice that for negative β the vertical displacement of the doublet will be larger and thus more sensitive to the details of these interactions.

V. CONCLUSIONS

We have studied the propulsion of micron-size elongated composites of paramagnetic colloidal doublets rotating close to a solid wall due to externally precessing magnetic fields. Direct propulsion of floating microscopic objects is achieved either by continuous actuation from outside (passive swimmer) or autonomous motion using some internal energy source (active swimmer). We have shown that undeformable colloidal composites change cyclically their distance to the plate during precession, with this being the clue to break time reciprocity because it takes advantage of the distance-dependent friction coefficient near a substrate. Our particularly simple model shows a mode of propulsion, which is particularly suited in confined geometries, as is the case in microfluidic environments and opens general perspectives for controlling micro-objects in confined fluids.

The actuated swimmer we have analyzed in detail differs from previous existing experimental realizations because it does not need to modify its shape and makes use of the two minimal independent degrees of freedom for propulsion i.e., displacements along and perpendicular to the bounding plate. The simplicity of the object has allowed us to identify the relevance of the bounding wall in order to identify the relevant degrees of freedom, which turn out to be specific to the particular mechanism that gives rise to self-propulsion. Actuated swimming due to a bounding wall differs in this respect from unbounded swimming due to body deformation or through a slip velocity on fixed shaped swimmers. We have shown that it is possible to optimize the system by using elliptic magnetic fields which induce rotations of the small particles closer to the solid wall and enhances the friction anisotropy induced by the bounding wall. Due to this reason, we believe that objects with anisotropic shapes will exhibit larger swimming velocity than their symmetric counterparts. Research in this direction employing different shape particles represents further direction of this work.

ACKNOWLEDGMENTS

P.T. was supported by the program "Juan de la Cierva" Grant No. JCI-2009–04192. P.T., O.G., and F.S. acknowledge financial support by MEC (Project No. FIS2006-03525) and DURSI (Grant No. 2005SGR00653). R.G. acknowledges support from the EPSRC. I.P. acknowledges financial support from MEC (Project No. FIS2008-04386) and DURSI (Grant No. 2005SGR00236).

[1] G. I. Taylor, Proc. R. Soc. London, Ser. A **209**, 447 (1951).
[2] S. Childress, *Mechanics of Swimming and Flying* (Cambridge University Press, Cambridge, England, 1981).
[3] See supplementary material at http://link.aps.org/supplemental/10.1103/PhysRevE.81.011402 for a video file showing the motion of one paramagnetic doublet subjected to an external precessing magnetic field with precession ratio 0.27 and frequency 81.7 s^{-1}.
[4] E. Lauga, Phys. Fluids **19**, 061703 (2007).
[5] T. Normand and E. Lauga, Phys. Rev. E **78**, 061907 (2008).
[6] E. M. Purcell, Am. J. Phys. **45**, 3 (1977).
[7] L. E. Becker, S. A. Koehler, and H. A. Stone, J. Fluid Mech. **490**, 15 (2003).

[8] D. Tam and A. E. Hosoi, Phys. Rev. Lett. **98**, 068105 (2007).
[9] A. Najafi and R. Golestanian, Phys. Rev. E **69**, 062901 (2004).
[10] D. J. Earl, C. M. Pooley, J. F. Ryder, I. Bredberg, and J. M. Yeomans, J. Chem. Phys. **126**, 064703 (2007).
[11] C. M. Pooley, G. P. Alexander, and J. M. Yeomans, Phys. Rev. Lett. **99**, 228103 (2007).
[12] R. Golestanian and A. Ajdari, Phys. Rev. Lett. **100**, 038101 (2008).
[13] G. P. Alexander and J. M. Yeomans, EPL **83**, 34006 (2008).
[14] J. E. Avron, O. Kenneth, and D. H. Oaknin, New J. Phys. **7**, 234 (2005).
[15] R. Dreyfus, J. Baudry, M. L. Roper, M. Fermigier, H. A. Stone, and J. Bibette, Nature (London) **437**, 862 (2005).
[16] R. Golestanian, T. B. Liverpool, and A. Ajdari, Phys. Rev. Lett. **94**, 220801 (2005).
[17] G. Ruckner and R. Kapral, Phys. Rev. Lett. **98**, 150603 (2007).
[18] V. Lobaskin, D. Lobaskin, and I. M. Kulic, Eur. Phys. J. Special Topics **157**, 149 (2008).
[19] Y.-G. Tao and R. Kapral, J. Chem. Phys. **128**, 164518 (2008).
[20] H. Morimoto, T. Ukai, Y. Nagaoka, N. Grobert, and T. Maekawa, Phys. Rev. E **78**, 021403 (2008).
[21] M. Iima and A. S. Mikhailov, EPL **85**, 44001 (2009).
[22] C. P. Lowe, FGCS, Future Gener. Comput. Syst. **17**, 853 (2001).
[23] E. Gauger and H. Stark, Phys. Rev. E **74**, 021907 (2006).
[24] M. Roper, R. Dreyfus, J. Baudry, M. Fermigier, J. Bibette, and H. A. Stone, J. Fluid Mech. **554**, 167 (2006).
[25] M. Roper, R. Dreyfus, J. Baudry, M. Fermigier, J. Bibette, and H. A. Stone, Proc. R. Soc. London, Ser. A **464**, 877 (2008).
[26] P. Garstecki, P. Tierno, D. B. Weibel, F. Sagués, and G. M. Whitesides, J. Phys.: Condens. Matter **21**, 204110 (2009).
[27] M. Belovs and A. Cebers, Phys. Rev. E **79**, 051503 (2009).
[28] W. F. Paxton, K. C. Kistler, C. C. Olmeda, A. Sen, S. K. S. Angelo, Y. Cao, T. E. Mallouk, P. E. Lammert, and V. H. Crespi, J. Am. Chem. Soc. **126**, 13424 (2004).
[29] J. R. Howse, R. A. L. Jones, A. J. Ryan, T. Gough, R. Vafabakhsh, and R. Golestanian, Phys. Rev. Lett. **99**, 048102 (2007).
[30] A. Snezhko, M. Belkin, I. S. Aranson, and W.-K. Kwok, Phys. Rev. Lett. **102**, 118103 (2009).
[31] S. T. Chang, V. N. Paunov, D. N. Petsev, and O. D. Velev, Nature Mater. **6**, 235 (2007).
[32] M. Leoni, J. Kotar, B. Bassetti, P. Cicuta, and M. C. Lagomarsino, Soft Matter **5**, 472 (2009).
[33] P. Tierno, R. Golestanian, I. Pagonabarraga, and F. Sagués, Phys. Rev. Lett. **101**, 218304 (2008).
[34] P. Tierno, R. Golestanian, I. Pagonabarraga, and F. Sagués, J. Phys. Chem. B **112**, 16528 (2008).
[35] S. Kim and S. J. Karrila, *Microhydrodynamics: Principles and Selected Applications* (Dover, New York, 2005).
[36] Y. W. Kim and R. R. Netz, J. Chem. Phys. **124**, 114709 (2006).
[37] J. W. Swan and J. F. Brady, Phys. Fluids **19**, 113306 (2007).
[38] B. Felderhof, Phys. Fluids **18**, 063101 (2006).
[39] H. A. Stone and A. D. T. Samuel, Phys. Rev. Lett. **77**, 4102 (1996).
[40] H. Zhang and M. Widom, Phys. Rev. E **51**, 2099 (1995).
[41] E. Helseth, J. Phys. D: Appl. Phys. **40**, 3030 (2007).
[42] L. Clime, B. L. Drogoff, and T. Veres, IEEE Trans. Magn. **43**, 2929 (2007).
[43] P. Tierno, S. Schreiber, W. Zimmermann, and T. M. Fischer, J. Am. Chem. Soc. **131**, 5366 (2009).
[44] S. H. Behrens and D. G. Grier, J. Chem. Phys. **115**, 6716 (2001).
[45] S. Lacis, J. C. Bacri, A. Cebers, and R. Perzynski, Phys. Rev. E **55**, 2640 (1997).